

RESEARCH PAPER



Synthesis and evaluation of AKR1C inhibitory properties of A-ring halogenated oestrone derivatives

Maša Sinreih^a, Rebeka Jójárt^b, Zoltán Kele^c, Tomaž Büdefeld^a, Gábor Paragi^{d,e}, Erzsébet Mernyák^b and Tea Lanišnik Rižner^a

^aFaculty of Medicine, Institute of Biochemistry and Molecular Genetics, University of Ljubljana, Ljubljana, Slovenia; ^bDepartment of Organic Chemistry, University of Szeged, Szeged, Hungary; ^cDepartment of Medicinal Chemistry, University of Szeged, Szeged, Hungary; ^dMTA-SZTE Biomimetic Systems Research Group, University of Szeged, Szeged, Hungary; ^eInstitute of Physics, University of Pécs, Pécs, Hungary

ABSTRACT

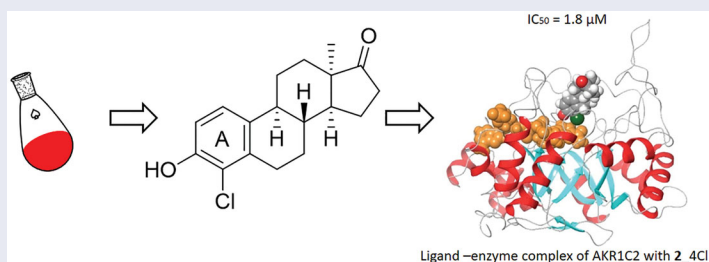
Enzymes AKR1C regulate the action of oestrogens, androgens, and progesterone at the pre-receptor level and are also associated with chemo-resistance. The activities of these oestrone halides were investigated on recombinant AKR1C enzymes. The oestrone halides with halogen atoms at both C-2 and C-4 positions (13 β -, 13 α -methyl-17-keto halogen derivatives) were the most potent inhibitors of AKR1C1. The lowest IC₅₀ values were for the 13 α -epimers **2**_2I,4Br and **2**_2I,4Cl (IC₅₀, 0.7 μ M, 0.8 μ M, respectively), both of which selectively inhibited the AKR1C1 isoform. The 13 α -methyl-17-keto halogen derivatives **2**_2Br and **2**_4Cl were the most potent inhibitors of AKR1C2 (IC₅₀, 1.5 μ M, 1.8 μ M, respectively), with high selectivity for the AKR1C2 isoform. Compound **1**_2Cl,4Cl showed the best AKR1C3 inhibition, and it also inhibited AKR1C1 (Ki: AKR1C1, 0.69 μ M; AKR1C3, 1.43 μ M). These data show that halogenated derivatives of oestrone represent a new class of potent and selective AKR1C inhibitors as lead compounds for further optimisations.

ARTICLE HISTORY

Received 18 February 2021
Revised 18 May 2021
Accepted 26 May 2021

KEYWORDS

Aldo-keto reductase; halogenated oestrone derivatives; inhibition; structure–activity relationships






Introduction


The enzymes of the aldo-keto reductase (AKR) superfamily catalyse NADPH-dependent reductions in carbonyl-group-containing substrates, to provide their alcohols¹. There are four human members of the AKR1C subfamily; AKR1C1–AKR1C3 are widely expressed, and AKR1C4 is liver specific. The AKR1C enzymes act as 3-keto, 17-keto, and 20-keto steroid reductases, through which they regulate the actions of androgens, oestrogens, and progestagens at the pre-receptor level². Differential expression of the genes that encode the AKR1C isoforms has been reported for a wide variety of cancers, including breast, prostate, and endometrial cancers, and also in benign pathologies, including endometriosis^{2–4}.

The AKR1C enzymes are associated with chemoresistance to platin-based drugs (e.g. cisplatin, carboplatin)^{5–8}, and they are also involved in resistance to the anthracycline chemotherapeutics daunorubicin, doxorubicin, idarubicin, and epirubicin^{9,10}. Studies

in model cell lines and in explant mouse models have shown that AKR1C inhibitors can reverse the chemoresistance in cervical, colon, bladder, and oral cancers, and that AKR1C3 inhibitors can restore cytotoxicity of daunorubicin and idarubicin in lung, liver, breast, and colon cancers, and in leukaemia cell lines^{9,11–17}. These actions of the AKR1C enzymes can be explained by their involvement in inactivation of cellular stressors, especially lipid peroxides, through reduction of 4-hydroxy-2-nonenal and inactivation of chemotherapeutics¹⁸.

The AKR genes are up-regulated by stress responses via the Nrf2–Keap1 pathway, which explains the overexpression of AKR1C1–AKR1C3 in chemoresistant cell lines and tumour samples¹⁸. Chemoresistance is the hallmark of cancers^{19,20}, and thus specific or pan-AKR1C inhibitors are needed to alleviate the serious and very frequent problems of resistance to platinum-based chemotherapeutics and individual anthracyclines.

CONTACT Tea Lanišnik Rižner tea.lanisnik-rizner@mf.uni-lj.si  Faculty of Medicine, Institute of Biochemistry and Molecular Genetics, University of Ljubljana, Vrazov trg 2, 1000 Ljubljana, Slovenia; Erzsébet Mernyák bobe@chem.u-szeged.hu  Department of Organic Chemistry, University of Szeged, Dóm tér 8., 6720 Szeged, Hungary; Gábor Paragi paragi@sol.cc.u-szeged.hu  MTA-SZTE Biomimetic Systems Research Group, University of Szeged, Dóm tér 8, Szeged H-6720, Hungary; Institute of Physics, University of Pécs, Ifjúság útja 6, Pécs H-7624, Hungary

 Supplemental data for this article can be accessed [here](#).

© 2021 The Author(s). Published by Informa UK Limited, trading as Taylor & Francis Group.

This is an Open Access article distributed under the terms of the Creative Commons Attribution-NonCommercial License (<http://creativecommons.org/licenses/by-nc/4.0/>), which permits unrestricted non-commercial use, distribution, and reproduction in any medium, provided the original work is properly cited.

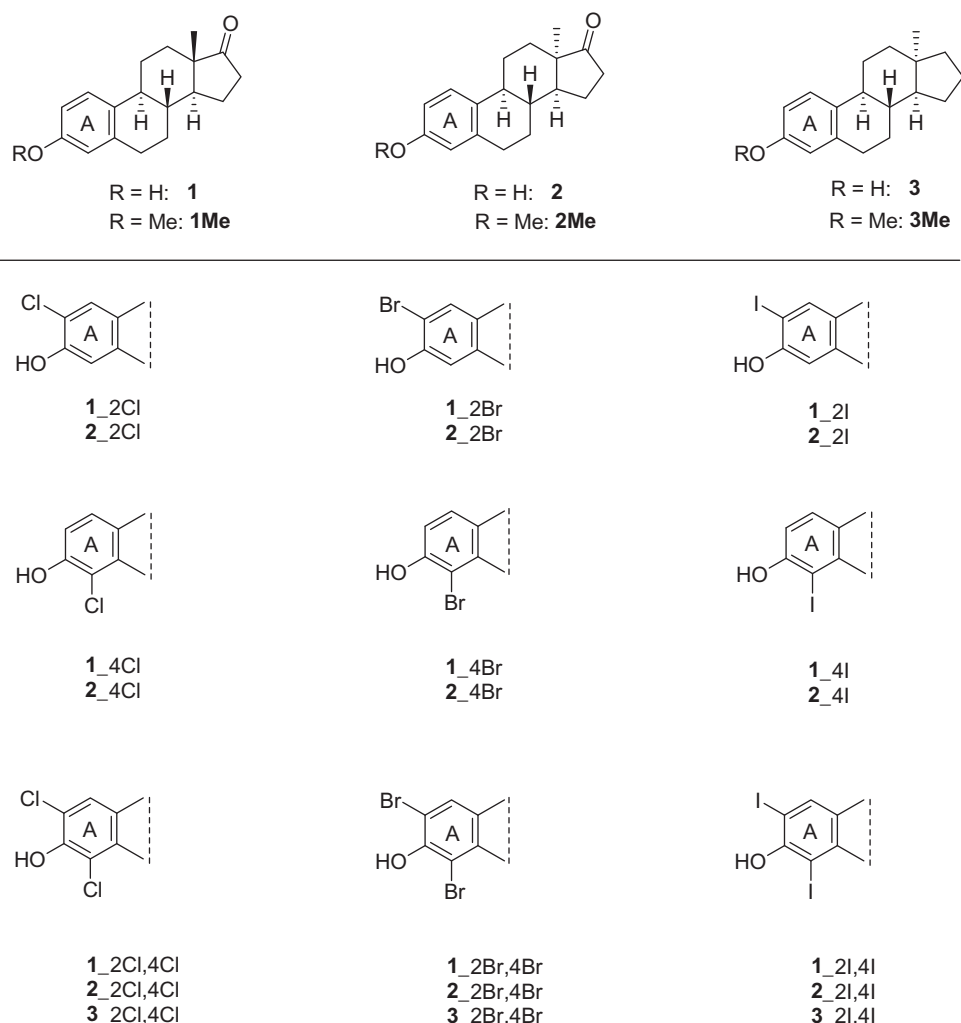


Figure 1. Structures of the oestrones and their halogenated derivatives considered in the present study.

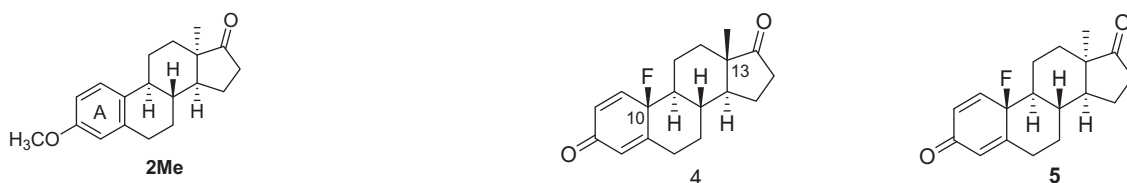


Figure 3. Structures of the epimeric 10-fluoro-1,4-dien-3-ones **4** and **5**.

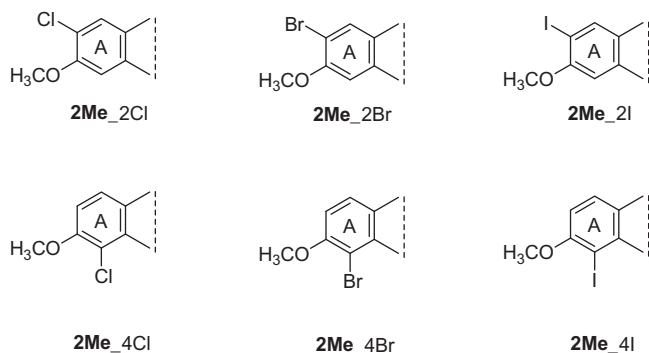


Figure 2. Structure of the halogenated 13 α -methyl-oestrone 3-methyl ethers considered in the present study.

Inhibitors against enzymes involved in the regulation of the actions of oestrogens at the pre-receptor level can be designed based on their oestrone substrates. However, one of the major

risks of oestrone-based inhibitors is their oestrogenic side-effects. This might be avoided by the use of core-modified synthetic oestrone derivatives that lack hormonal activity. Owing to its modified conformation, 13 α -oestrone meets these requirements, in terms of low affinity for nuclear oestrogen receptors^{21,22}. We reported recently on the synthesis and biochemical assessment of oestrone A-ring halogenated derivatives (Figures 1 and 2)^{23–25}. The 2- and 4-halogenated, and the 2,4-bis-halogenated derivatives were subjected to biochemical investigations into their effects on the enzymes involved in oestrogen biosynthesis. Important structure–activity relationships were defined, and certain potent inhibitors of 17 β -hydroxysteroid dehydrogenase 1 and steroid sulphatase were identified²⁵.

Previous transformation of substrates **1** and **2** (Figures 1 and 2) with Selectfluor as reagent produced the 10 β -fluoro-oestra-1,4-dien-3-ones (Figure 3)²⁶. The 10-fluoro and 10-chloro 13-epimeric 1,4-dien-3-ones have also been investigated for inhibition of the

human aromatase enzyme, which is responsible for aromatisation of androgens to oestrogens²⁶. For this aromatase, the 13 β -methyl group of these compounds appeared to be crucial, as only the 13 β -methyl compounds were potent inhibitors, with submicromolar or micromolar IC₅₀ values.

Several halogenated 13 α -methyl-oestrones have been evaluated for inhibition of organic anion transporting polypeptide 2B1 (OATP2B1), which is involved in cellular transport of oestrone sulphate²⁴. The OATP2B1 inhibitory potential greatly depended on the structure of the tested derivative. The most potent derivative showed outstanding OATP2B1 inhibition with submicromolar IC₅₀. Considering all of the available data for these A-ring halogenated derivatives, and especially those of 13 α -oestrone, this compound group appears to be particularly promising for the design of anti-tumoral agents with multiple inhibitory actions. Furthermore, based on our recent data, structurally different enzymes might be inhibited by the same synthetic compounds.

With these considerations in mind, we aimed here to investigate the inhibitory properties against the enzymes AKR1C1–3 of the recently and newly synthesised halogenated derivatives of oestrone. The test compound set included the 13 β -methyl-oestrone (**1**) and 13 α -methyl-oestrone (**2**) halogenated derivatives and the 17-deoxy-13 α -methyl (**3**) counterparts, with the halogens at C-2 and/or C-4. Additional to the investigations of these base compounds, a selection of their 3-methoxy derivatives (**1Me**, **2Me**, **3Me**) and the 13-epimeric 10-fluoro 1,4-dien-3-ones (**4**, **5**) were halogenated and included. Finally, for selected ligands, computational investigations were used to gain insight into the molecular backgrounds of the enzyme selectivities using docking and molecular dynamics (MD). On the assumption that greater biological activity can be achieved through stronger ligand–protein interactions, the ligands with well-defined selectivities were considered for each enzyme. Concerning specific interactions, the selected ligands and the enzymes were analysed initially by docking calculations and then by MD.

Materials and methods

Chemistry

Melting points were determined with a Kofler hot-stage apparatus, and are uncorrected. Elemental analysis was performed with an organic elemental analyser (2400 CHN; Perkin-Elmer, Waltham, MA). Thin-layer chromatography was run on silica gel 60 F254 plates (layer thickness, 0.2 mm; Merck, Darmstadt, Germany) with 30% ethyl acetate/70% hexane as eluent. Detection was with I₂ or UV light (365 nm) after spraying with 5% phosphomolybdic acid in 50% aqueous phosphoric acid, and heating to 100–120 °C for 10 min. Flash chromatography was run on silica gel 60 plates (40–63 μ m; Merck, Darmstadt, Germany). ¹H nuclear magnetic resonance (NMR) spectra were recorded in dimethylsulphoxide (DMSO)-d₆ or CDCl₃ solution (DRX-500; Bruker, Billerica, MA) at 500 MHz, with Me₄Si as internal standard. ¹³C NMR spectra were recorded with the same instrument at 125 MHz, and under the same conditions. Mass spectrometry provided the full scan mass spectra of the compounds using a triple quadrupole mass spectrometer (TSQ-7000; Finnigan-MAT, San Jose, CA), and were acquired in the range of 50 *m/z* to 1000 *m/z*, using an electrospray ionisation source (Finnigan, San Jose, CA). The analyses were performed in negative ion mode using flow injection mass spectrometry, with a mobile phase of 50% aqueous acetonitrile. The flow rate was 0.3 mL/min. Five microlitre aliquots of the samples were loaded into the flow. The electrospray ionisation capillary

was adjusted to 4.5 kV, and N₂ was used as the nebuliser gas. The oestrone derivatives were synthesised as described elsewhere, except for those bearing different halogens at positions C-2 and C-4^{23,27}.

Synthesis of 2-bromo-4-chloro-3-hydroxy-13 α -oestra-1,3,5(10)-trien-17-one (**2_2Br,4Cl**) and 4-bromo-2-chloro-3-hydroxy-13 α -oestra-1,3,5(10)-trien-17-one (**2_2Cl,4Br**)

4-Chloro-13 α -methyl-oestrone **2_4Cl** (152 mg, 0.50 mmol) or 2-chloro-13 α -methyl-oestrone **2_2Cl** (152 mg, 0.50 mmol) was dissolved in dichloromethane (5 mL), and *N*-bromosuccinimide (0.50 mmol) was added. The mixture was stirred at room temperature for 2 h, the solvent was evaporated off, and the crude product **2_2Br,4Cl** or **2_2Cl,4Br** was subjected to flash chromatography, with 10% ethyl acetate/90% hexane as eluent.

Product **2_2Br,4Cl** (175 mg, 91%) was obtained as an oil. R_f=0.46. Anal Calcd. for C₁₈H₂₀BrClO₂: C, 56.34; H, 5.75. Found C, 56.47, H, 5.82%. ¹H NMR (DMSO-d₆) δ ppm: 0.96 (s, 3H, H-18), 2.55 and 2.81 (2xm, 2x1H, H-6), 7.38 (s, 1H, H-1), 9.64 (s, 1H, 3-OH). ¹³C NMR (DMSO-d₆) δ ppm: 20.4 (CH₂), 24.4 (C-18), 27.1 (CH₂), 27.9 (CH₂), 28.1 (CH₂), 31.4 (CH₂), 32.8 (CH₂), 40.6 (CH), 48.1 (2C, 2x CH), 49.2 (C-13), 108.8 (C), 121.9 (C), 128.3 (C-1), 134.0 (C), 135.0 (C), 147.4 (C-3), 220.5 (C-17). MS: [M-H]⁻ 381 (35Cl/79Br) and 383 (35Cl/81Br).

Product **2_2Cl,4Br** (171 mg, 89%) was obtained as an oil. R_f=0.46. Anal Calcd. for C₁₈H₂₀BrClO₂: C, 56.34; H, 5.75. Found C, 56.49, H, 5.84%. ¹H NMR (DMSO-d₆) δ ppm: 0.96 (s, 3H, H-18), 2.56 and 2.82 (2xm, 2x1H, H-6), 7.38 (s, 1H, H-1), 9.65 (s, 1H, 3-OH). ¹³C NMR (DMSO-d₆) δ ppm: 20.4 (CH₂), 24.4 (C-18), 27.1 (CH₂), 27.9 (CH₂), 28.1 (CH₂), 31.4 (CH₂), 32.8 (CH₂), 40.6 (CH), 48.1 (2C, 2x CH), 49.2 (C-13), 108.8 (C), 121.9 (C), 128.3 (C-1), 134.1 (C), 135.0 (C), 147.5 (C-3), 220.5 (C-17). MS: [M-H]⁻ 381 (35Cl/79Br) and 383 (35Cl/81Br).

Synthesis of 4-chloro-3-hydroxy-2-iodo-13 α -oestra-1,3,5(10)-trien-17-one (**2_2I,4Cl**) and 2-chloro-3-hydroxy-4-iodo-13 α -oestra-1,3,5(10)-trien-17-one (**2_2Cl,4I**)

4-Chloro-13 α -methyl-oestrone **2_4Cl** (152 mg, 0.50 mmol) or 2-chloro-13 α -methyl-oestrone **2_2Cl** (152 mg, 0.50 mmol) was dissolved in trifluoroacetic acid (5 mL), and *N*-iodosuccinimide (0.50 mmol) was added. The mixture was stirred at room temperature for 2 h, and then poured into 100 mL water, and extracted with dichloromethane. The organic phase was separated, neutralised with ammonia solution, and washed with a saturated solution of sodium thiosulphate in water. The organic phase was dried over anhydrous sodium sulphate, filtered, and evaporated. The crude product was subjected to flash chromatography with 10% ethyl acetate/90% hexane as eluent.

Product **2_2I,4Cl** (198 mg, 92%) was obtained as an oil. R_f=0.50. Anal Calcd. for C₁₈H₂₀ClIO₂: C, 50.19; H, 4.68. Found C, 50.26, H, 4.78%. ¹H NMR (DMSO-d₆) δ ppm: 0.96 (s, 3H, H-18), 2.56 and 2.82 (2xm, 2x1H, H-6), 7.55 (s, 1H, H-1), 9.64 (s, 1H, 3-OH). ¹³C NMR (DMSO-d₆) δ ppm: 20.4 (CH₂), 24.4 (C-18), 27.2 (CH₂), 28.0 (CH₂), 28.2 (CH₂), 31.4 (CH₂), 32.8 (CH₂), 37.1 (CH₂), 40.5 (CH), 48.1 (2C, 2x CH), 49.2 (C-13), 84.1 (C-4), 120.3 (C-2), 134.2 (C-1), 134.9 (C), 135.7 (C), 149.8 (C-3), 220.5 (C-17). MS *m/z* (%): 429 (100, [M-H]⁻).

Product **2_2Cl,4I** (194 mg, 90%) was obtained as an oil. R_f=0.52. Anal Calcd. for C₁₈H₂₀ClIO₂: C, 50.19; H, 4.68. Found C, 50.27, H, 4.76%. ¹H NMR (DMSO-d₆) δ ppm: 0.96 (s, 3H, H-18), 2.56 and 2.75 (2xm, 2x1H, H-6), 7.30 (s, 1H, H-1), 9.75 (s, 1H, 3-OH).

^{13}C NMR (DMSO- d_6) δ ppm: 20.4 (CH₂), 24.3 (C-18), 28.1 (CH₂), 28.3 (CH₂), 31.5 (CH₂), 32.8 (CH₂), 37.1 (CH₂), 40.9 (CH), 48.1 (2C, 2x CH), 49.3 (C-13), 96.2 (C), 117.2 (C), 126.8 (C-1), 134.2 (C), 139.2 (C), 149.6 (C-3), 220.5 (C-17). MS m/z (%): 429 (100, [M-H]⁻).

Synthesis of 4-bromo-3-hydroxy-2-iodo-13 α -oestra-1,3,5(10)-trien-17-one (2_2I,4Br) and 2-bromo-3-hydroxy-4-iodo-13 α -oestra-1,3,5(10)-trien-17-one (2_2Br,4I)

4-Bromo-13 α -methyl-oestrone **2_4Br** (174 mg, 0.50 mmol) or 2-bromo-13 α -methyl-oestrone **2_2Br** (174 mg, 0.50 mmol) was dissolved in trifluoroacetic acid (5 mL), and *N*-iodosuccinimide (0.50 mmol) was added. The mixture was stirred at room temperature for 2 h, and then poured into 100 mL water and extracted with dichloromethane. The organic phase was separated, neutralised with ammonia solution, and washed with a saturated solution of sodium thiosulphate in water. The organic phase was dried over anhydrous sodium sulphate, filtered, and evaporated. The crude product was subjected to flash chromatography with 10% ethyl acetate/90% hexane as eluent.

Product **2_2I,4Br** (216 mg, 91%) was obtained as an oil. $R_f=0.50$. Anal Calcd. for C₁₈H₂₀BrIO₂: C, 45.50; H, 4.24. Found C, 45.62, H, 4.33%. ^1H NMR (DMSO- d_6) δ ppm: 0.96 (s, 3H, H-18), 2.56 and 2.76 (2xm, 2x1H, H-6), 7.59 (s, 1H, H-1), 9.41 (s, 1H, 3-OH). ^{13}C NMR (DMSO- d_6) δ ppm: 20.4 (CH₂), 24.4 (C-18), 27.5 (CH₂), 28.1 (CH₂), 31.5 (CH₂), 32.8 (CH₂), 39.5 (CH), 40.5 (CH), 48.1 (CH), 49.2 (C-13), 84.4 (C-2), 113.6 (C-4), 135.0 (C-1), 135.6 (C-10), 137.4 (C-5), 150.6 (C-3), 220.5 (C-17). MS: [M-H]⁻ 472 (79Br) and 474 (81Br).

Product **2_2Br,4I** (221 mg, 93%) was obtained as an oil. $R_f=0.52$. Anal Calcd. for C₁₈H₂₀BrIO₂: C, 45.50; H, 4.24. Found C, 45.60, H, 4.30%. ^1H NMR (DMSO- d_6) δ ppm: 0.96 (s, 3H, H-18), 2.54 and 2.73 (2xm, 2x1H, H-6), 7.43 (s, 1H, H-1), 9.52 (s, 1H, 3-OH). ^{13}C NMR (DMSO- d_6) δ ppm: 20.4 (CH₂), 24.3 (C-18), 28.2 (CH₂), 28.3 (CH₂), 31.5 (CH₂), 32.8 (CH₂), 37.2 (CH₂), 40.8 (CH), 48.1 (2C, 2x CH), 49.3 (C-13), 96.7 (C-2), 107.3 (C-4), 129.9 (C-1), 134.9 (C-10), 139.9 (C-5), 150.5 (C-3), 220.5 (C-17). MS: [M-H]⁻ 472 (79Br) and 474 (81Br).

Inhibition assays for the AKR1C enzymes

The AKR1C-3 recombinant enzymes were prepared as described previously²⁸. The *in vitro* catalytic activities of AKR1C-3 were determined spectrophotometrically by measuring increased NADH absorbance ($\epsilon_{340}=6220 \text{ M}^{-1} \text{ cm}^{-1}$) in the presence of the chiral artificial substrate 1-acenaphthenol. The enzymatic reactions (300 μL) were performed in 0.09 M potassium phosphate buffer (pH 9.0), 0.005% (v/v) Triton X-114, 0.05% (v/v) DMSO, 2.3 mM NAD⁺, and 1-acenaphthenol (all Sigma). The final substrate concentrations (i.e. 1-acenaphthenol) were 90 μM , 180 μM , and 250 μM , for AKR1C1, AKR1C2, and AKR1C3, respectively. Five microlitres of each tested compound in DMSO was added to the reaction mixture, with the reactions started by addition of the enzymes, at 0.1 μM , 0.3 μM , and 1.5 μM for AKR1C1, AKR1C2, and AKR1C3, respectively. The measurements were performed in duplicate and were repeated as two independent experiments, using a microplate reader (PowerWave XS; Biotek, Winooski, VT). The initial velocities were calculated and the IC₅₀ values were determined from the plots of residual activity (RA) versus log₁₀ (inhibitor concentration), using GraphPad Prism, version 7.00 (GraphPad Software, Inc., San Diego, CA). Type of inhibition, K_M , K_i , and α were determined using either GraphPad Prism, version 7.00 (GraphPad Software, Inc., San Diego, CA) or SigmaPlot, version 14.0 (Systat Software, Inc., San Jose, CA).

Computer simulation

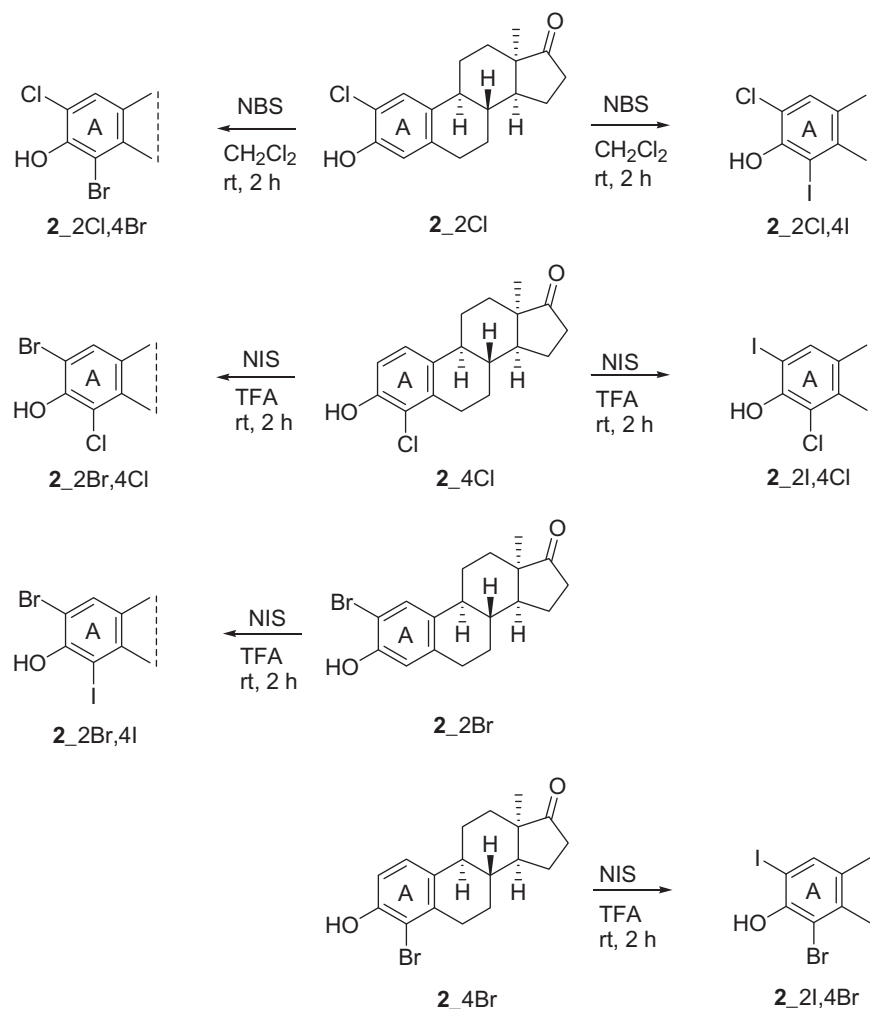
Docking calculations were performed with the Glide programme^{29–31} from the Schrodinger suite³², using the XP protocol. Docking grid generation was based on the X-ray crystal geometry from the protein database (<http://www.rcsb.org>), and the graphical user interface Protein Preparation Wizard tool in Maestro³³ was applied to determine the positions of the missing hydrogens, side chains, and loops. The Protein Preparation Wizard step was augmented with 5-ns-long MD running with the Desmond module³⁴ from the Schrodinger suite³². The last frame of the MD calculation was considered as the target protein in the docking investigations. The XP docking protocol was applied in each case with the enhanced sampling method, and the energy window for the ring sampling was also increased to 100 kcal/mol, and the number of final outputs per ligand was increased to 10. Following the docking calculations, the best docking pose of each ligand was considered as the starting structure for a 500-ns-long MD simulation. To calculate the binding free energy (ΔG) of the ligand-protein complex, the molecular mechanics generalised Born surface area (MMGBSA) method was applied for each MD trajectory, for 2500 dynamic trajectory points. The OPLS3e force field and simple point charge water model were applied in all of the MD calculations, and the MMGBSA values were determined by the *thermal_mmgsa* python script from the Schrodinger suite. Standard error of means and mean ΔG values of a complex were determined by bootstrap calculations using an in-house script, where 100,000 bootstrap iterations were performed with eight randomly selected datapoints from the ΔG values. All of the figures were prepared with the Maestro programme³³, which is the GUI part of the Schrodinger programme package.

Results and discussion

Synthesis of the halogenated derivatives of oestrone

Electrophilic substitutions with *N*-halosuccinimides were carried out in our recent studies, starting from the 13 β -methyl-oestrone (**1**), its 13 α -methyl epimer (**2**) and the 17-deoxy-13 α -methyl-oestrone (**3**; Figure 2)^{26,27}. Halogenations occurred at the *ortho* positions relative to the phenolic OH group. Mono-substituted and *bis*-substituted derivatives were formed. Starting from the 3-methyl ethers (**1Me**, **2Me**, **3Me**), mono-halogenated derivatives were obtained exclusively. Some of these halogenated oestrone derivatives showed potent inhibition of aromatase, oestrone sulphatase, and 17 β -hydroxysteroid dehydrogenase, and/or OATP2B1 actions^{26,27}. Important structure-activity relationships were identified. These studies indicated that the 13 α -methyl epimer of the natural oestrone might be superior to its 13 β -methyl counterpart, as it is readily available and hormonally inactive and has other promising biological properties. The group of 2,4-*bis* halogenated compounds provided the most promising inhibitors from the biological point of view.

Encouraged by these data, we continued our interest in the synthesis of A-ring halogenated derivatives of 13 α -methyl-oestrone here. 2,4-Disubstituted compounds that included different halogens were synthesised (Scheme 1). The order of the halogen introduction had to be defined, whereby the smaller halogen had to be introduced first. Chlorination of 13 α -methyl-oestrone (**2**) resulted in the 2-chloro and 4-chloro derivatives, which were subjected to bromination. The 4-bromo-2-chloro (**2_2Cl,4Br**) and 2-bromo-4-chloro (**2_2Br,4Cl**) compounds were obtained in high yields. Iodination of the chloro derivatives led to the 2-chloro-4-iodo (**2_2Cl,4I**) and 4-chloro-2-iodo (**2_2I,4Cl**) derivatives. *Bis*



Scheme 1. Synthesis of the 2,4-disubstituted 13 α -methyl-oestrone derivatives with the different halogens.

compounds that included bromo and iodo substituents were synthesised starting from the 2-bromo and 4-bromo substrates. Iodination with *N*-iodosuccinimide provided the desired 2-bromo-4-iodo (**2_2Br,4I**) and 4-bromo-2-iodo (**2_2I,4Br**) products in excellent yields.

Halogenated derivatives of oestrone inhibit the AKR1C enzymes

Along with the three starting oestrones (**1**, **2**, **3**) and their 3-methyl ether derivatives (**1Me**, **2Me**, **3Me**), we evaluated 35 halogenated derivatives of oestrone as inhibitors of the recombinant enzymes AKR1C1, AKR1C2, and AKR1C3. There were 29 13 α -methyl-oestrones, which included 3-hydroxy,17-keto-oestrones (16 compounds), 3-methoxy, 17-keto-oestrones (seven compounds) and 17-deoxy-oestrones (five compounds). There were also 12 13 β -methyl-17-keto-oestrones. The screening data for these oestrones and their derivatives for inhibition of recombinant enzymes AKR1C1-AKR1C3 are presented in Table 1.

Initial screening at 100 μ M oestrones revealed that a number of these acted as potent inhibitors: 13 compounds showed $\geq 80\%$ inhibition of AKR1C1 (six compounds at 10 μ M), 11 compounds showed $\geq 80\%$ inhibition of AKR1C2 (six compounds at 10 μ M), and 10 compounds showed $\geq 80\%$ inhibition of AKR1C3 (none at 10 μ M). When the compounds were screened at 10 μ M, additional potent inhibitors of AKR1C2 were revealed that had shown lower

inhibitory activities at the higher concentration (**1_4Br**, **1_4Cl**, **2_2Br**), which was probably caused by solubility issues.

Among the 13 β -methyl-17-keto-oestrones, five showed potent inhibition of AKR1C1, as $\geq 80\%$ at 100 μ M, with IC_{50} values for the two most promising compounds, **1_2Br,4Br** and **1_2Cl,4Cl**, of 5.4 μ M and 1.6 μ M, respectively. Neither of these two were selective inhibitors of AKR1C1, as **1_2Br,4Br** also showed strong inhibition of AKR1C2 (IC_{50} =5.6 μ M), and **1_2Cl,4Cl**, of AKR1C3 (IC_{50} =6.3 μ M). Two other 13 β -methyl-17-keto oestrones, **1_4Br** and **1_4Cl**, inhibited AKR1C2 in the low micromolar range (IC_{50} =7.0, 5.3 μ M, respectively), while no inhibition was seen for these at 10 μ M with AKR1C1, and low inhibition was seen for AKR1C3 (25% and 50%, respectively).

The 13 α -methyl-17-keto-oestrones in the 3-methyl ether series generally showed weaker inhibition of the AKR1C enzymes compared to their 3-hydroxy counterparts. Indeed, only two of these showed inhibition $\geq 80\%$ at 100 μ M, for AKR1C3 (**2Me_2Cl**, **2Me_4Cl**), with much weaker inhibition of AKR1C1 and AKR1C2. The more potent inhibition by the 13 α -methyl-17-keto-oestrones in the 3-hydroxy series included six compounds with $\geq 80\%$ inhibition of AKR1C1 at 10 μ M, where the best two had IC_{50} of 0.7 μ M and 0.8 μ M (**2_2I,4Br**, **2_2I,4Cl**, respectively). Five of these compounds inhibited AKR1C2 by $\geq 80\%$ at 10 μ M, where the best inhibitor had an IC_{50} of 1.5 μ M (**2_2Br**). This group of oestrone derivatives did not include any potent AKR1C3 inhibitors (i.e. none $\geq 80\%$ inhibition at 10 μ M).

Table 1. Inhibition of the AKR1C enzymes by the halogenated oestrone derivatives.

Compound	AKR1C1			AKR1C2			AKR1C3		
	Inhibition (%)		IC ₅₀ /Ki (μM)	Inhibition (%)		IC ₅₀ /Ki (μM)	Inhibition (%)		IC ₅₀ /Ki (μM)
100 μM	10 μM	100 μM		10 μM	100 μM		10 μM		
1	10.0	NI		50.0	NI		NI	NI	
1Me	22.5	8.2		70.0	4.8		NI	16.7	
1_2I	22.5	31.3		52.5	20.2		NI	NI	
1_4I	10.0	8.3		NI	NI		NI	36.4	
1_2I,4I	25.0	42.2		62.2	21.3		NI	13.6	
1_2Br	65.0	51.2		25.0	36.4		40.2	13.0	
1_4Br	100.0	NI		62.5	73.0	7.0	8.3	25.0	
1_2Br,4Br	82.5	67.0	5.4	99.8	83.0	5.6	58.3	50.0	
1_2Cl	91.6	50.0		88.0	53.0		86.8	NI	
1_4Cl	80.0	NI		25.0	70.0	5.3	91.7	50.0	
1_2Cl,4Cl	94.8	46.9	1.6/0.69	50.0	23.4		90.4	21.9	6.3, 1.43
2	22.5	7.5		65.0	3.5		29.8	22.5	
2Me	20.0	1.3		35.0	NI		59.9	22.9	
2_2I	42.5	37.8		50.0	22.4		NI	33.8	
2_4I	22.5	2.3		75.0	16.5		85.7	35.1	12.3
2_2I,4I	77.5	NI		45.0	NI		50.0	2.6	
2_2Br	22.5	47.2		65.0	81.4	1.5	23.8	62.6	
2_4Br	14.2	NI		98.3	80.0	2.2	58.2	25.0	
2_2Br,4Br	88.7	82.5	5.3	86.0	70.3	7.3	50.8	27.9	
2_2Cl	45.1	50.0		75.4	83.0	2.1	72.3	60.0	8.7
2_4Cl	22.5	18.5		80.0	73.9	1.8	43.6	5.3	
2_2Cl,4Cl	95.9	84.8	2.8	81.5	84.1	4.6	89.8	69.9	12.8
2_2I,4Br	93.4	90.7	0.7/0.57	74.7	59.5		43.6	40.0	
2_2I,4Cl	99	90.0	0.8	87.5	73.0	7.1	72.2	50.0	
2_2Br,4I	100	67.0	7.2	100	75.0	4.4	88.9	50.0	
2_2Br,4Cl	92.3	80.0	1.7	99.0	80.0	3.1	89.4	50.0	
2_2Cl,4I	82.6	50.0		89.2	73.0	4.6	58.0	NI	
2_2Cl,4Br	93.9	80.0	1.9	91.9	65.0		88.0	25.0	
2Me_2Br	NI	7.1		NI	NI		18.3	13.6	
2Me_4Br	12.5	12.9		15.0	NI		39.7	44.6	
2Me_2I	NI	1.0		5.0	NI		50.8	NI	
2Me_4I	NI	5.1		NI	NI		19.8	NI	
2Me_2Cl	35.7	17.0		76.3	60.0		91.0	60.0	
2Me_4Cl	21.4	NI		78.8	50.0		90.0	50.0	
3	12.5	13.8		NI	NI		NI	23.4	
3Me	NI	NI		75.0	NI		49.2	21.1	
3_2Cl,4Cl	2.8	39.4		76.8	66.2		44.6	NI	
3_2Br,4Br	64.3	33.0		74.4	68.0	0.9/1.98	26.7	50.0	
3_2I,4I	9.8	17.5		11.7	22.9		27.3	11.4	
4	25.0	NI		30.0	NI		NI	NI	
5	50.0	7.1		75.0	10.5		41.7	24.1	

NI: no inhibition.

Data in bold, compounds showing $\geq 80\%$ inhibition for the respective AKR1C.

Finally, we screened five 13α -methyl-17-deoxy derivatives. For the initial testing at $100\ \mu\text{M}$, some promising results were shown, but only for AKR1C2 (three compounds showed around 75% inhibition). At $10\ \mu\text{M}$, **3_2Br,4Br** and **3_2Cl,4Cl** showed 68.0% and 66.2% inhibition, respectively, with the best compound, **3_2Br,4Br**, with an IC₅₀ of $0.9\ \mu\text{M}$.

To further evaluate these oestrone derivatives as inhibitors of the AKR1C enzymes, we conducted detailed kinetic studies on three different compounds, which were chosen as they were the most potent inhibitors of AKR1C1, AKR1C2, and AKR1C3. The first was compound **1_2Cl,4Cl**, or *bis*-chloro- 13β -methyl-17-keto-oestrone, which inhibited both AKR1C1 and AKR1C3 potently, but showed low inhibition of AKR1C2. These inhibition studies revealed a mixed type of inhibition of **1_2Cl,4Cl** for AKR1C1 (Ki = $0.69\ \mu\text{M}$), which was instead competitive for inhibition of AKR1C3 (Ki = $1.43\ \mu\text{M}$) (Table S1). The second compound chosen here was **2_2I,4Br**, a 3-hydroxy disubstituted 13α -methyl-17-keto-oestrone, which at $10\ \mu\text{M}$ showed 90.7% inhibition of AKR1C1, 59.5% inhibition of AKR1C2 and 40.0% of AKR1C3. Its IC₅₀ for AKR1C1 was $0.7\ \mu\text{M}$, with Ki of $0.57\ \mu\text{M}$. Here, **2_2I,4Br** showed a mixed type of inhibition of AKR1C1. Finally, the third compound chosen was **3_2Br,4Br**, a 13α -methyl-17-deoxy *bis*-bromo oestrone, which

showed selectivity for AKR1C2, with IC₅₀ of $0.9\ \mu\text{M}$. **3_2Br,4Br** also showed mixed type of inhibition, with Ki of $1.98\ \mu\text{M}$.

Structure–activity relationships

On the basis of these inhibition data, we were able to postulate the initial structure–activity relationship for all three AKR1C isoforms. The most potent of these AK1C1 inhibitors were a 13β -methyl-17-keto-oestrone (**1_2Cl,4Cl**) and a 13α -methyl-17-keto-oestrone (**2_2I,4Br**), with the halogen atoms at both C-2 and C-4 (Figure 4). For the 13β -methyl-17-keto-oestrone, the activity was highest with bromine and chlorine, which indicated that iodine would probably be too large, and would result in lower enzyme inhibition. Here, the most potent inhibitor had chlorine at both positions, for its IC₅₀ of $1.6\ \mu\text{M}$. For the equivalent 13α -methyl epimers, the lowest IC₅₀ were achieved with iodine on C-2 and bromine or chlorine on C-4 (IC₅₀: **2_2I,4Br**, $0.7\ \mu\text{M}$; **2_2I,4Cl**, $0.8\ \mu\text{M}$). These oestrone derivatives were selective for AKR1C1. The loss of the 17-keto group (**3**, and its derivatives) or methylation of the 3-hydroxy group (**2Me**, **3Me**, and their derivatives) had negative impact on the AKR1C inhibition.

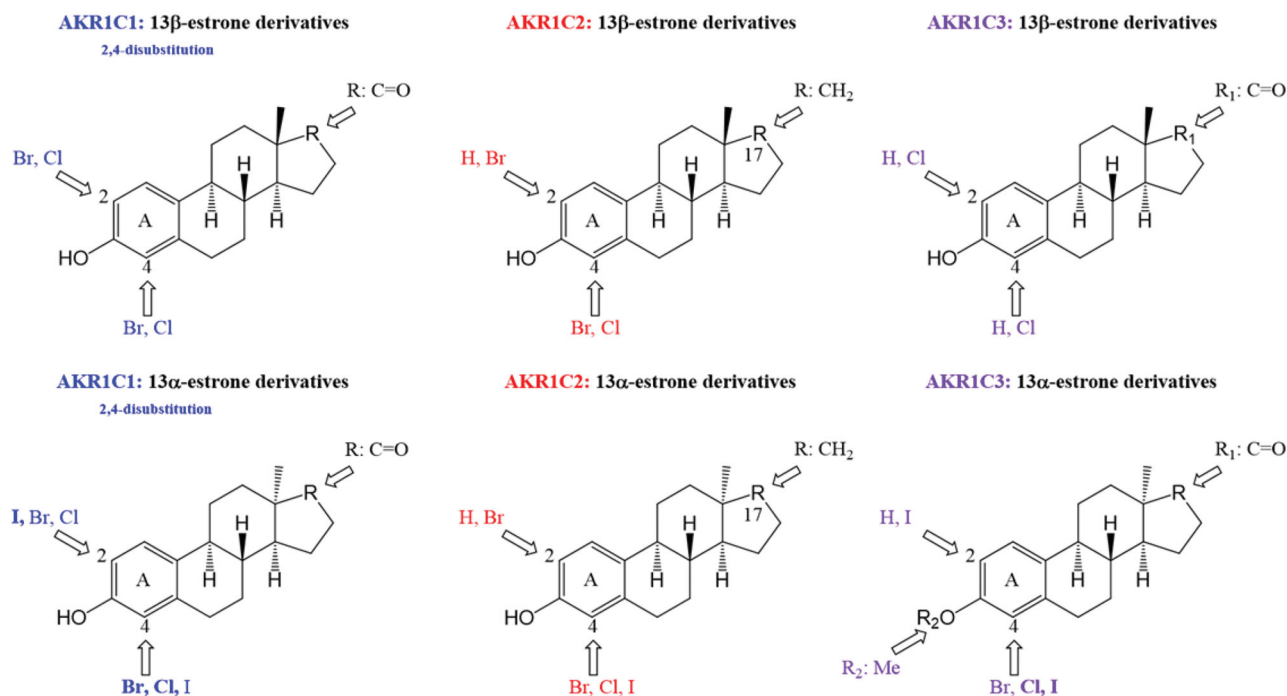


Figure 4. Structure–activity relationship for inhibition of the AKR1C1-3 enzymes.

We established here that with the 13β -methyl epimers, no substitution or bromine substitution at C-2 was effective for inhibition of AKR1C2, while bromine or chlorine at C-4 was beneficial, but not iodine (Figure 4). The larger halogens at C-4 thus appeared to be advantageous. The loss of the keto group at position 17 halved the IC_{50} . The best two AKR1C2 inhibitors among the 13α -methyl-17-keto-estrone epimers had only a bromine at the C-2 position and only a chlorine at the C-4 position (IC_{50} : **2_2Br**, $1.5\ \mu\text{M}$; **2_4Cl**, $1.8\ \mu\text{M}$). These two compounds also showed high selectivity for the AKR1C2 isoform.

These structure–activity relationship studies also revealed that chlorine substitution of 13β -methyl-17-keto estrones at C-2 and/or C-4 was required for AKR1C3 inhibition, with improvement for both at the same time (IC_{50} : **1_2Cl,4Cl**, $6.3\ \mu\text{M}$; Figure 4). With bromine substitution showing low inhibition of AKR1C3, all inhibition was lost with either no substitution or iodine substitution. For 13α -methyl-3-methoxy-17-keto-estrone, bromine or chlorine substitution at C-2 and the larger halogens at C-4 (i.e. chlorine, iodine) were required for AKR1C3 inhibition, while this inhibition of AKR1C3 was almost completely lost when the 17-keto group was removed. Methylation of 3-hydroxy group greatly improved the potency of the AKR1C3 inhibition.

Computational simulations

For an atomic level investigation of the structural background of the biological activities, computational simulations were carried out for the ligands that showed well-defined enzyme selectivities. First, docking calculations were performed using the Glide programme^{29–31}, where receptor models were based on experimental X-ray crystal structures from the PDB database (<http://www.rcsb.org>). The following structures were selected for AKR1C1, AKR1C2, and AKR1C3: 1MRQ (AKR1C1 in complex with NADPH and 20α -hydroxyprogesterone); 4L1W (AKR1C2 in complex with NADP^+ and progesterone); and 1XF0 (AKR1C3 in complex with NADP^+ and androstenedione). The structures were prepared for docking calculations according to the details in the “Materials and methods”

section. It is worth noting that various structures can be retrieved for each enzyme in the PDB database, but the crystal structures were always selected here, with co-crystallisation with a steroid ligand.

The precision of the docking protocol was verified by redocking the original crystal ligand into the binding pocket, where the XP method with the applied settings accurately reproduced the binding poses of the original co-crystallised ligands. Then, all the selected ligands (**2_2I,4Br**, **2_4Cl**, **2_4I**) were docked into each relaxed target, where the scoring function of the docking program (glide-score) correlates with the binding free energy (ΔG) and therefore with the enzyme activity. Unfortunately, even the ligand with the highest biological activity for the relevant receptor could not be properly predicted by the docking calculations (see Glide score values in Table 2).

Thus, a more advanced ΔG calculation scheme was applied, namely the MMGBSA method, which used 500-ns-long MD trajectories for all the nine ligand–target complexes. The starting structures of the MD simulations were always the best pose geometries from the docking calculations, and the MMGBSA binding free energies were computed as 2500 snapshots for each trajectory. Statistical descriptors were calculated for all the nine ligand–target complexes, including means and standard error of means of ΔG , with these data shown in Table 2. It can be seen that the MMGBSA calculations always defined the most active ligand and with the strongest binding affinity for each enzyme. So, these 500-ns-long MD simulations can correctly represent the ligand–target interactions. It can also be mentioned that the tertiary structures of the three enzymes were very similar; each of them contained a central β -barrel structure that was surrounded by eight α -helices and a nicotine-adenosine-diphosphate co-factor on one of the tops of the barrel. The steroid binding site was located on the top side of the β -barrel, adjacent to the co-factor. The binding pocket was formed by flexible loops in all three cases, which emphasises the dynamic nature of the ligand binding. On the basis of these impressions of the binding geometry of a steroid in an AKR1C enzyme, we have presented here the starting

Table 2. Scoring values of docking calculations, mean and standard error of means (SEM) of binding energies (in kcal/mol) determined by MMGBSA calculations, as well as biological inhibition (at 100 μ M) for the tested compounds are presented.

Compound	Glide score			ΔG_{MMGBSA}						Biological activity		
	AKR1C1	AKR1C2	AKR1C3	AKR1C1		AKR1C2		AKR1C3		AKR1C1	AKR1C2	AKR1C3
				Mean	SEM	Mean	SEM	Mean	SEM			
2_2I,4Br	-8.3	-7.8	-8.4	-60.3	3.5	-57.7	1.7	-55.8	4.0	93.4	74.7	43.6
2_4Cl	-8.7	-8.5	-7.9	-55.5	1.6	-59.9	1.6	-56.1	2.5	22.5	80.0	43.6
2_4I	-8.4	-8.2	-7.3	-53.8	1.9	-52.7	1.83	-72.1	2.0	22.5	75.0	85.7

The enzyme structures in docking studies were based on X-ray crystal structures from the pdb database (<http://www.rcsb.org>; AKR1C1, 1MRQ; AKR1C2, 4L1W; AKR1C3, 1XF0).

poses of the MD calculations for all of the three ligands in their "preferred" enzyme in the [Supplementary Information \(Figure S1\)](#).

As the MMGBSA calculations successfully identified the most active ligands as the strongest binding ones, we examined all of the nine 500-ns-long trajectories using the Simulation Interaction Diagram tool from the Schrodinger suite. Here, among the other analyses, the protein–ligand interaction diagram was obtained in each case, where the occurrence of all of the important interactions were determined along the trajectories concerned (hydrogen bonds, hydrophobic interactions, water bridges, etc.). Moreover, the positions of the significant interactions on the ligands were also demonstrated in simplified 2D diagrams ([Supplementary Figures S2–S4](#), boxed insets), as shown together with the interaction diagrams in the Supporting Information ([Figures S2–S4](#)).

Comparisons were also made between the interaction diagrams of the selective compounds and the diagrams of the less active compounds at each enzyme. However, neither a new secondary bond formation nor a unique interaction that might be solely responsible for the selectivity were found for any of the enzymes. It seemed that the patterns of the different interactions can help to explain the possible sources of the selectivity here. For example, for AKR1C1, the π - π stacking of the A-ring of compound **2_2I,4Br** and the significant hydrophobic interactions, as well as the largest number of water-bridge connections, might together have resulted in **2_2I,4Br** having the strongest interaction with the AKR1C1 enzyme ([Supplementary Figure S2](#)). For AKR1C2, with **2_4Cl**, the greater hydrophobic interactions with residue Trp86 and the larger number of water bridges might together override the similar interaction patterns of **2_4I** and **2_2I,4Br**, although these last two also show extra π - π stacking ([Supplementary Figure S3](#)). Finally, for AKR1C3, the stable interaction of the keto-oxygen in the D-ring with residue Ser118, and the less stable, but probably stronger, interaction with the negatively charged residue Asp224 might have been responsible for the strong binding.

In summary here, we can say that there was no formation of new hydrogen or halogen bonds with the flexible loops that might have been responsible for the selectivity, although hydrophobic interactions might have particularly important roles in the selectivities of these compounds. Hence, the variations of atoms at positions 2 and 4 in the sterane skeletons might fine-tune these effects.

Conclusions

The AKR1C enzymes are promising drug targets, as they are involved in the development of different cancers and several benign pathologies, and they are also associated with chemoresistance to platin and anthracycline-based drugs. Here, we synthesised 35 halogenated oestrone derivatives with low affinities for the nuclear oestrogen receptors, and evaluated their inhibitory actions against AKR1C1, AKR1C2, and AKR1C3. Some potent

inhibitors were identified, with occasional dual or triple inhibitory properties. Selective compounds were found against each of these three enzymes. Atomic level computational simulations showed that neither a well-defined unique chemical connection nor a specific interaction with a single amino acid could be identified in search of a source of selectivity regarding potent ligands. Overall, these data indicate that these halogenated oestrones represent a new class of potent and selective AKR1C inhibitors, and thus have the potential for development of new antitumour agents.

Acknowledgements

The authors thank Ajda Godec and Anastazija Zajec for help with enzyme inhibition assays, and Špela Kos for technical support.

Disclosure statement

The authors report no conflict of interest.

Funding

The work of Erzsébet Mernyák on this project was supported by the János Bolyai Research Scholarship of the Hungarian Academy of Sciences. This work was supported by the National Research, Development and Innovation Office-NKFIH through project OTKA SNN 124329 and project N1-0066 from the Slovenian Research Agency.

References

1. Penning TM. The aldo-keto reductases (AKRs): overview. *Chem Biol Interact* 2015;234:236–46.
2. Rizner TL, Penning TM. Role of aldo-keto reductase family 1 (AKR1) enzymes in human steroid metabolism. *Steroids* 2014;79:49–63.
3. Hevir N, Vouk K, Sinkovec J, et al. Aldo-keto reductases AKR1C1, AKR1C2 and AKR1C3 may enhance progesterone metabolism in ovarian endometriosis. *Chem Biol Interact* 2011;191:217–26.
4. Rizner TL, Penning TM. Aldo-keto reductase 1C3-assessment as a new target for the treatment of endometriosis. *Pharmacol Res* 2020;152:104446.
5. Shiiba M, Yamagami H, Yamamoto A, et al. Mefenamic acid enhances anticancer drug sensitivity via inhibition of aldo-keto reductase 1C enzyme activity. *Oncol Rep* 2017;37: 2025–32.
6. Matsumoto R, Tsuda M, Yoshida K, et al. Aldo-keto reductase 1C1 induced by interleukin-1 β mediates the invasive

- potential and drug resistance of metastatic bladder cancer cells. *Sci Rep* 2016;6:34625.
7. Matsunaga T, Hojo A, Yamane Y, et al. Pathophysiological roles of aldo-keto reductases (AKR1C1 and AKR1C3) in development of cisplatin resistance in human colon cancers. *Chem Biol Interact* 2013;202:234–42.
 8. Chen CC, Chu CB, Liu KJ, et al. Gene expression profiling for analysis acquired oxaliplatin resistant factors in human gastric carcinoma TSGH-S3 cells: the role of IL-6 signaling and Nrf2/AKR1C axis identification. *Biochem Pharmacol* 2013;86: 872–87.
 9. Hofman J, Malcekova B, Skarka A, et al. Anthracycline resistance mediated by reductive metabolism in cancer cells: the role of aldo-keto reductase 1C3. *Toxicol Appl Pharmacol* 2014;278:238–48.
 10. Plebuch M, Soldan M, Hungerer C, et al. Increased resistance of tumor cells to daunorubicin after transfection of cDNAs coding for anthracycline inactivating enzymes. *Cancer Lett* 2007;255:49–56.
 11. Hintzpetter J, Seliger JM, Hofman J, et al. Inhibition of human anthracycline reductases by emodin – a possible remedy for anthracycline resistance. *Toxicol Appl Pharmacol* 2016;293: 21–9.
 12. Veitch ZW, Guo B, Hembruff SL, et al. Induction of 1C aldo-ketoreductases and other drug dose-dependent genes upon acquisition of anthracycline resistance. *Pharmacogenet Genomics* 2009;19:477–88.
 13. Heibein AD, Guo B, Sprowl JA, et al. Role of aldo-keto reductases and other doxorubicin pharmacokinetic genes in doxorubicin resistance, DNA binding, and subcellular localization. *BMC Cancer* 2012;12:381–10.
 14. Novotna E, Bukum N, Hofman J, et al. Roscovitine and purvalanol A effectively reverse anthracycline resistance mediated by the activity of aldo-keto reductase 1C3 (AKR1C3): a promising therapeutic target for cancer treatment. *Biochem Pharmacol* 2018;156:22–31.
 15. Matsunaga T, Yamaguchi A, Morikawa Y, et al. Induction of aldo-keto reductases (AKR1C1 and AKR1C3) abolishes the efficacy of daunorubicin chemotherapy for leukemic U937 cells. *Anticancer Drugs* 2014;25:868–77.
 16. Verma K, Zang T, Gupta N, et al. Selective AKR1C3 inhibitors potentiate chemotherapeutic activity in multiple acute myeloid leukemia (AML) cell lines. *ACS Med Chem Lett* 2016;7: 774–9.
 17. Verma K, Zang T, Penning TM, Trippier PC. Potent and highly selective aldo-keto reductase 1C3 (AKR1C3) inhibitors act as chemotherapeutic potentiators in acute myeloid leukemia and T-cell acute lymphoblastic leukemia. *J Med Chem* 2019;62:3590–616.
 18. Penning TM. Aldo-keto reductase regulation by the Nrf2 system: implications for stress response, chemotherapy drug resistance, and carcinogenesis. *Chem Res Toxicol* 2017;30: 162–76.
 19. Brasseur K, Gevry N, Asselin E. Chemoresistance and targeted therapies in ovarian and endometrial cancers. *Oncotarget* 2017;8:4008–42.
 20. Ji X, Lu Y, Tian H, et al. Chemoresistance mechanisms of breast cancer and their countermeasures. *Biomed Pharmacother* 2019;114:108800.
 21. Schonecker B, Lange C, Kottteritzsch M, et al. Conformational design for 13 α -steroids. *J Org Chem* 2000;65:5487–97.
 22. Ayan D, Roy J, Maltais R, Poirier D. Impact of estradiol structural modifications (18-methyl and/or 17-hydroxy inversion of configuration) on the in vitro and in vivo estrogenic activity. *J Steroid Biochem Mol Biol* 2011;127:324–30.
 23. Bacsa I, Jojart R, Schneider G, et al. Synthesis of A-ring halogenated 13 α -estrone derivatives as potential 17 β -HSD1 inhibitors. *Steroids* 2015;104:230–6.
 24. Laczko-Rigo R, Jojart R, Mernyak E, et al. Structural dissection of 13-epiestrones based on the interaction with human organic anion-transporting polypeptide, OATP2B1. *J Steroid Biochem Mol Biol* 2020;200:105652.
 25. Bacsa I, Herman BE, Jojart R, et al. Synthesis and structure-activity relationships of 2- and/or 4-halogenated 13 β - and 13 α -estrone derivatives as enzyme inhibitors of estrogen biosynthesis. *J Enzyme Inhib Med Chem* 2018;33:1271–82.
 26. Jojart R, Traj P, Kovacs E, et al. Synthesis, biological evaluation and docking studies of 13-epimeric 10-fluoro- and 10-chloroestra-1,4-dien-3-ones as potential aromatase inhibitors. *Molecules* 2019;24:1783.
 27. Hong Y, Chen S. Aromatase, estrone sulfatase, and 17 β -hydroxysteroid dehydrogenase: structure-function studies and inhibitor development. *Mol Cell Endocrinol* 2011;340: 120–6.
 28. Brozic P, Smuc T, Gobec S, Rizner TL. Phytoestrogens as inhibitors of the human progesterone metabolizing enzyme AKR1C1. *Mol Cell Endocrinol* 2006;259:30–42.
 29. Friesner RA, Banks JL, Murphy RB, et al. Glide: a new approach for rapid, accurate docking and scoring. 1. Method and assessment of docking accuracy. *J Med Chem* 2004;47: 1739–49.
 30. Friesner RA, Murphy RB, Repasky MP, et al. Extra precision glide: docking and scoring incorporating a model of hydrophobic enclosure for protein-ligand complexes. *J Med Chem* 2006;49:6177–96.
 31. Halgren TA, Murphy RB, Friesner RA, et al. Glide: a new approach for rapid, accurate docking and scoring. 2. Enrichment factors in database screening. *J Med Chem* 2004;47:1750–9.
 32. Schrödinger. Schrödinger release 2020–4. New York (NY): Schrödinger LLC; 2020.
 33. Maestro S. Schrödinger release 2020–3. New York (NY): Schrödinger LLC; 2020.
 34. DESR. Desmond molecular dynamics system, Schrödinger release 2020–3. Maestro-Desmond interoperability tools. New York (NY): Schrödinger; 2020.